



CHORUS

This is the accepted manuscript made available via CHORUS. The article has been published as:

High- T_c superconductivity in $\text{CaKFe}_4\text{As}_4$ in absence of nematic fluctuations

W.-L. Zhang, W. R. Meier, T. Kong, P. C. Canfield, and G. Blumberg

Phys. Rev. B **98**, 140501 — Published 10 October 2018

DOI: [10.1103/PhysRevB.98.140501](https://doi.org/10.1103/PhysRevB.98.140501)

High T_c superconductivity in $\text{CaKFe}_4\text{As}_4$ in absence of nematic fluctuations

W.-L. Zhang,^{1,*} W. R. Meier,^{2,3} T. Kong,^{2,3} P. C. Canfield,^{2,3} and G. Blumberg^{1,4,†}

¹*Department of Physics & Astronomy, Rutgers University, Piscataway, New Jersey 08854, USA*

²*Department of Physics and Astronomy, Iowa State University, Ames, Iowa 50011, USA*

³*Division of Materials Science and Engineering, Ames Laboratory, Ames, Iowa 50011, USA*

⁴*National Institute of Chemical Physics and Biophysics, Akadeemia tee 23, 12618 Tallinn, Estonia*

(Dated: September 17, 2018)

We employ polarization-resolved Raman spectroscopy to study multi-band stoichiometric $T_c=35$ K superconductor $\text{CaKFe}_4\text{As}_4$. We do not detect Pomeranchuk-like electronic nematic fluctuations which were universally observed in XY (B_{2g}) symmetry Raman response for most families of the Fe-based superconductors. In the superconducting state we observe consistent with nodeless order parameter full spectral weight suppression at low energies and emergence of a composite pair-breaking coherence feature at energies between 12 and 20 meV. We analyze the superconductivity induced phonon self-energy effects and give an estimation for the electron-phonon coupling constant $\lambda^\Gamma=0.0015$ which is insufficient to provide attraction for high T_c pairing.

Introduction – Understanding the pairing mechanism in the Fe-based superconductors (FeSCs) remains in a focus of research not only due to a high superconducting transition temperature T_c , but also because of the interplay of superconductivity with other electronic degrees of freedom, nematicity and magnetism in particular [1–6].

Electronic nematicity has been universally observed for many families of FeSCs [7, 8]. Furthermore, compositions that are in proximity to the nematic quantum critical point (QCP) often show the highest T_c [7–11]. The T_c enhancement near QCP scenario was recently studied by several theoretical proposals [12–14].

Raman spectroscopy has been often used to study the superconducting (SC) order parameter [11, 15–19], the dynamics of electronic nematic fluctuations [10, 11, 20, 21], as well as the electron-phonon interactions [22–25]. The FeSCs are well suited to study the mechanisms of T_c enhancement from an experimental point of view.

Recent discovery of a new class of stoichiometric and strictly tetragonal superconductors $\text{CaAFe}_4\text{As}_4$ ($A = \text{K, Rb, Cs}$) with rather high T_c (31-36 K) provides an ideal platform for spectroscopic investigation of FeSCs in a clean limit, and to decide if the nematicity is a necessary condition for high T_c superconductivity in FeSCs [26–30]. Although the pristine $\text{CaAFe}_4\text{As}_4$ compounds do not show a long range magnetic order, an electron doping *via* substitution of Co or Ni for Fe, and/or application of pressure, suppresses T_c and induces an exotic spin-vortex crystal order, while the system remains tetragonal even for the magnetically ordered phase [31–33].

Crystallographic structure – The $\text{CaKFe}_4\text{As}_4$ structure may be considered as a modification of the extensively studied tetragonal 122 family of FeSCs with the body-centered structure $I4/mmm$. For $\text{CaKFe}_4\text{As}_4$, every other plane of Ca atom is replaced by K, reducing the crystallographic space group to primitive $P4/mmm$ (point group D_{4h}) and therefore doubling the number of atoms in the primitive cell. In Figs. 1(a-b) we compare the tetragonal CaFe_2As_2 and $\text{CaKFe}_4\text{As}_4$ lattices.

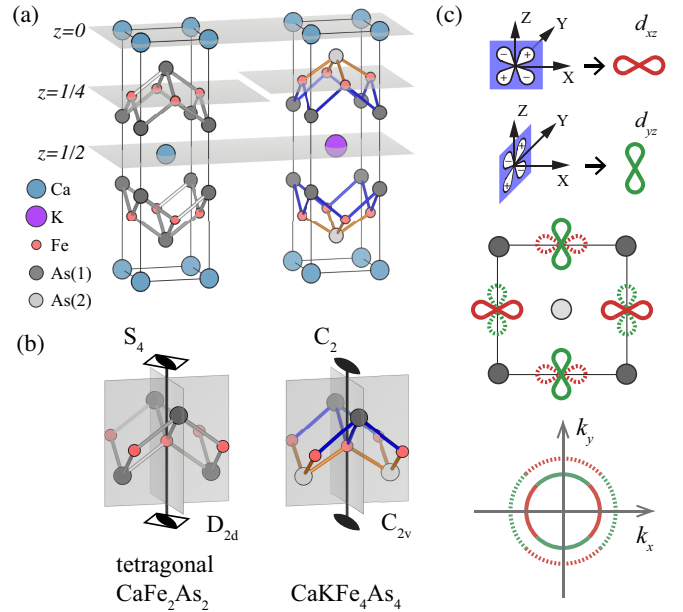


FIG. 1. (a) The comparison between CaFe_2As_2 and $\text{CaKFe}_4\text{As}_4$ lattice structures. For $\text{CaKFe}_4\text{As}_4$, the Fe sites are shifted away from the high symmetry $z=1/4$ and $3/4$ planes, causing two distinct As-Fe bond distances (shown in blue and orange). (b) The reduction of the Fe site-symmetry from D_{2d} for CaFe_2As_2 to C_{2v} for $\text{CaKFe}_4\text{As}_4$. (c) For $\text{CaKFe}_4\text{As}_4$, a sketch of the partially occupied d_{xz}/d_{yz} orbital order (the upper panel for real space), and derived two FS pockets in the vicinity of the Γ point (the lower panel for momentum space). Solid and dotted lines denote differences in the orbital occupation which induce a static quadrupole moment on the Fe sites with a checkerboard order.

For the body-centered CaFe_2As_2 structure the Fe layers are confined to the high symmetry $z=1/4$ and $3/4$ planes. All the Fe positions have D_{2d} site-symmetry with S_4 axis along z-direction, which imposes the degeneracy condition for Fe $3d_{xz}$ and $3d_{yz}$ orbitals. Such orbital degeneracy is a common feature for most of FeSC structures [34, 35].

It has been conjectured that degeneracy of the par-

tially filled d_{xz}/d_{yz} orbitals is a necessary condition for anomalously strong nematic effects in FeSCs: such degeneracy enables dynamical charge oscillations in sub-THz frequency range giving rise to fluctuating charge ferro-quadrupole moment with an amplitude proportional to the local oscillating charge imbalance $n_{xz} - n_{yz}$ [11]. The soft ferro-quadrupole fluctuations often show critical behavior leading to a d -wave Pomeranchuk-like instability [11]. These fluctuations most dramatically manifest themselves in the low-frequency part of XY -symmetry Raman response as an overdamped quasi-elastic feature in the normal state [10, 11, 20] which undergoes a metamorphosis into a coherent in-gap collective mode below T_c [11, 17–19, 37, 38].

In contrast to doped CaFe_2As_2 -structure-like $\text{Ba}_{1-x}\text{K}_x\text{Fe}_2\text{As}_2$ where K^+ substitute ions randomly occupy the host Ba^{2+} sites, for $\text{CaKFe}_4\text{As}_4$ the Ca^{2+} and K^+ ions are ordered in two distinct layers above and below Fe-As layers. This layering of $\text{Ca}^{2+}/\text{K}^+$ ions causes the planes of Fe ions shift vertically away from the high symmetry positions [39, 40]. The shift results in nonequivalent Fe-As bond distances for the As atoms above and below the Fe layer, thus, the Fe site symmetry is reduced from D_{2d} to C_{2v} , Fig. 1(a-b).

The removal of the S_4 symmetry on the Fe sites takes away the degeneracy of the partially occupied Fe d_{xz}/d_{yz} orbitals [39], which gives rise to a static charge imbalance between these two orbitals, and, hence, creates a static $d_{x^2-y^2}$ -symmetry quadrupole moment on each Fe site. Because the orbital character of the lower energy state flips between the two neighboring Fe sites, the structure forms a static checkerboard anti-quadrupole order, Fig. 1(c). The stiffness of the static anti-quadrupole order parameter precludes Pomeranchuk-like fluctuations for the $\text{CaKFe}_4\text{As}_4$ compound.

In this work we study the charge dynamics in $\text{CaKFe}_4\text{As}_4$ single-crystals by polarization-resolved Raman spectroscopy. We demonstrate that in contrast to the data from many FeSCs for which strong Pomeranchuk-like electronic nematic fluctuations which give rise to intense electronic Raman continuum in the XY -quadrupole symmetry channel, the electronic Raman signal for $\text{CaKFe}_4\text{As}_4$ is isotropic and generally weak. This data indeed support the notion that the quadrupole fluctuations for $\text{CaKFe}_4\text{As}_4$ structure are quenched. Below T_c , we observe complete suppression of the low-frequency spectral intensity indicating that all FS pockets are fully gapped, and transfer of the spectral weight to a composite SC coherence feature between 12 and 20 meV in the XY symmetry electronic Raman response. We also observe superconductivity induced phonon self-energy effect and estimate the electron-phonon (e-p) coupling to be weak, with coupling constant $\lambda^{\Gamma} = 0.0015$.

Experimental – Polarization-resolved Raman scattering measurements were performed in quasi-back scattering geometry from the natural cleaved (001) surface. We

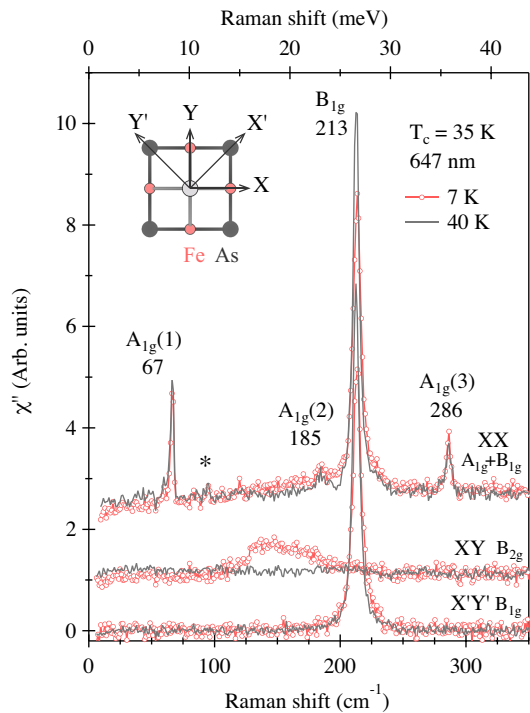


FIG. 2. Raman spectra for single crystal $\text{CaKFe}_4\text{As}_4$ at 40 and 7 K. The XY and XX polarized spectra are offset by 1 and 2 units, respectively. Inset: top view of the Fe-As layer and axes notation.

use $\mu\nu = XX, XY$ and $X'Y'$ scattering geometries [41]. These geometries allow coupling to $A_{1g}+B_{1g}$, B_{2g} and B_{1g} symmetry excitations correspondingly.

The $\text{CaKFe}_4\text{As}_4$ single crystals ($T_c = 35$ K) used in this study were synthesized by flux method [26, 28]. The crystals were loaded into a continuous helium flow optical cryostat immediately after being cleaved in a connected to the cryostat nitrogen gas glove bag. For excitation we used the 647 nm line of a Kr^+ laser, where the laser beam was focused to a $50 \times 50 \mu\text{m}$ spot. The laser power was kept below 10 mW in the normal state and 2.3 mW in the SC state. All referred temperatures are corrected for the laser heating. The Raman signal was collected and analyzed by a triple-grating spectrometer with 1.5 cm^{-1} spectral resolution. Spectra were corrected for spectral response and background determined from the $X'Y'$ symmetry electronic continuum to obtain the Raman scattering intensity $I_{\mu\nu}(\omega, T)$ [42]. The Raman response function was derived as $\chi''_{\mu\nu}(\omega, T) = I_{\mu\nu}(\omega, T)/[1 + n(\omega, T)]$, here $n(\omega, T)$ is the Bose distribution factor.

Raman continuum and the superconducting gap – In Fig. 2 we compare Raman response above and below T_c for three polarizations. Above T_c , besides four sharp phonon modes, spectra show a weak featureless electronic continuum for all polarizations. For the XX and $X'Y'$ scattering geometries, the electronic continuum shows surprisingly little change across T_c , while for XY po-

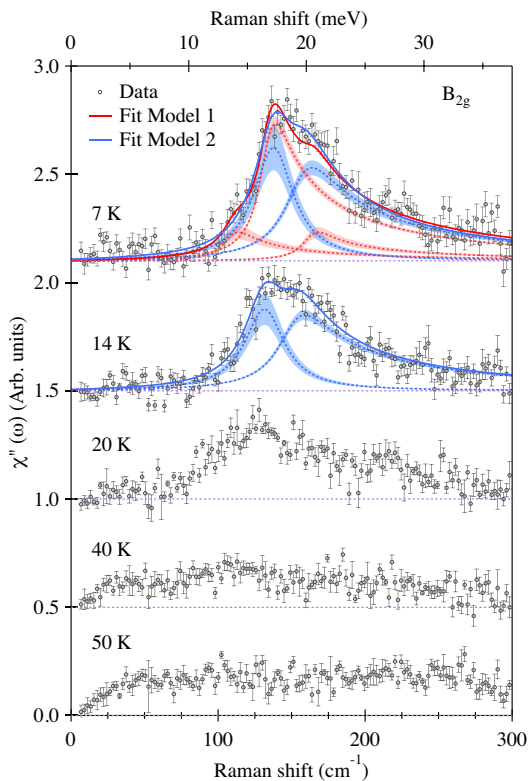


FIG. 3. (a) Temperature evolution of the Raman response in B_{2g} channel. Error bars show one standard deviation. Red lines denote a model fit with three isotropic gap function [15, 43]. Another model fit comprising of an isotropic gap and a shallow collective mode is shown in blue. The decompositions are shown by dotted lines, where shadings denote one standard deviation error.

larization below T_c the low-frequency spectral weight is transferred to a broad composite feature between 12 to 30 meV (100 to 240 cm^{-1} , Fig. 3), which we relate to formation of the SC gap on multiple FS pockets [15, 44]. Upon cooling, the intensity of this feature growth, while the spectral intensity below 12 meV is completely suppressed at 7 K, implying that the SC gap is nodeless. We do not observe any sharp in-gap resonance modes below the composite gap feature.

For a multi-band system the composite structure of the SC coherence feature could arise due to an overlap of several pair-breaking coherence peaks corresponding to gap values at different FS pockets [45]. An additional structure could also arise due to gap anisotropy on each FS pocket, or due to appearance of a shallow in-gap collective mode [16, 44, 46, 47]. The collective mode could be caused by interactions both in particle-particle or in particle-hole channels [11, 17, 18, 37, 38, 46, 48].

In Fig. 3 we fit the low temperature data and compare two models:

- The first model (shown in red), which conforms to the ARPES data [45], is comprised of three pair-breaking co-

herence peaks due to isotropic gaps on three FS pockets i : $\chi'' = \sum_{i=1}^3 \alpha_i \chi_i''$. Here $\chi_i''(\omega, \Delta_i, T) = 4\Delta_i^2/\omega\sqrt{\omega^2 - 4\Delta_i^2} * L(\omega, T)$ denotes BCS coherence peaks with SC gap energies $2\Delta_i$ convoluted with $L(\omega, T)$ that accounts for temperature and instrumental broadening, and α_i denotes the weight of Raman coupling [15, 43].

- The second model (in blue) is comprised of a collective mode (CM) due to electron-hole or particle-particle attraction in d_{xy} -symmetry channel and a single pair-breaking coherence peak.

The energies resulted from the models are collected in Table I. The models are difficult to tell apart solely based on the Raman data. However, the second model is hard to reconcile with one-electron spectroscopy data [45], and even if the second model containing a CM would apply, the interactions in the sub-dominant d_{xy} -wave channel cannot be strong because the mode's small binding energy. This is in contrast to $\text{Ba}_{1-x}\text{K}_x\text{Fe}_2\text{As}_2$ at optimal doping [18, 19], or to Na-111 [11] for which sharp in-gap CMs with significant binding energy have been reported.

Phonon self-energy effects – $\text{CaKFe}_4\text{As}_4$ crystal (point group D_{4h}) contains 10 atoms in a primitive cell. For the Γ point phonons, group-theoretical symmetry decomposition yields $A_u + E_u$ acoustic modes, $4A_{2u} + 5E_u$ infrared active modes, $3A_{1g} + B_{1g} + 4E_g$ Raman active modes, and a B_{2u} silent mode. For the scattering experiments from the (001) surface, we observe all the three A_{1g} and a B_{1g} phonons (Fig. 2). The phonon energies and atomic displacements are summarized in Table II.

Above T_c all modes exhibit a conventional temperature dependence: hardening and narrowing upon cooling due to anharmonic decay [49–51]. However, we note that the behavior for the B_{1g} phonon mode in the SC state is anomalous: the mode's energy and line width increase upon cooling, as shown in Fig. 4(a).

Similar phonon anomalies upon entering into SC state were reported for MgB_2 [25] and for cuprate superconductors [22, 23, 52–55]. The behavior was explained by Zeyher-Zwicknagl's model [24] which implies that in the presence of electron-phonon coupling, phonon self-energy is upward renormalized when the SC gap opens and the electronic density-of-states is pushed to the proximity of the phonon mode above the gaps energies.

It is interesting to note that in contrast to the 67 cm^{-1} A_{1g} phonon (Fig. 2) that exhibits an asymmetric Fano line shape, the B_{1g} phonon shows nearly perfect Lorentzian shape. We attribute this to weak Raman coupling to the B_{1g} symmetry electronic continuum: the

TABLE I. Summary of fitting result at 7 K, units in meV

Model 1: three SC gaps	Model 2: CM+SC gap
$\Delta_1 = 13.6 \pm 0.6$	$\omega_{CM} = 16.4 \pm 0.21$
$\Delta_2 = 16.8 \pm 0.1$	$\Delta_1 = 18.9 \pm 0.4$
$\Delta_3 = 20.2 \pm 0.2$	

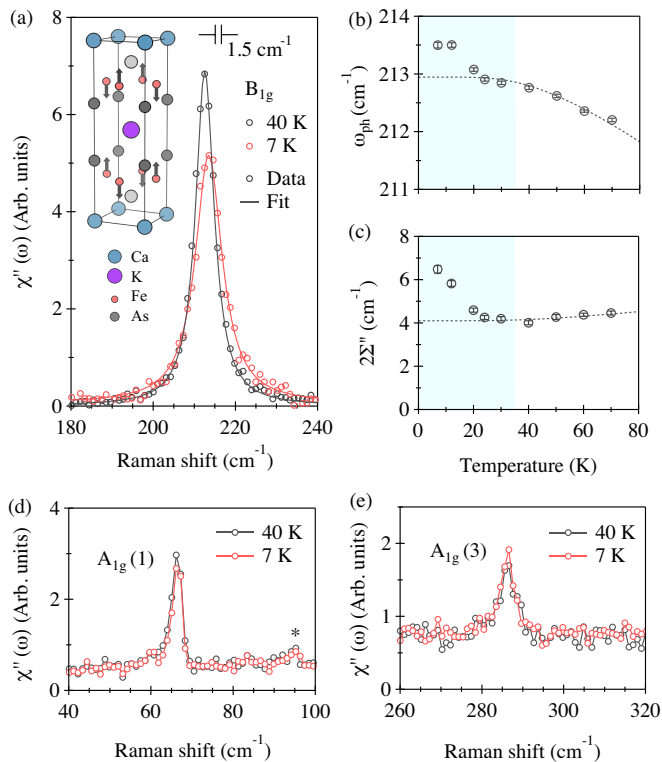


FIG. 4. Temperature evolution of phonon spectra. (a) The B_{1g} phonon spectra and the fitting curve for above (40 K) and below (7 K) T_c . Inset of (a): Atomic displacements of the B_{1g} phonon. (b)-(c) Temperature dependence of B_{1g} phonon energy ω_{ph} and line width $2\Sigma''$. Σ'' has been corrected for the spectrometer resolution as shown in (a). Dashed lines describe the anharmonic decay into two phonons obtained from the fit for the normal state. (d)-(e) The $A_{1g}(1)$ and $A_{1g}(3)$ phonon modes at 40 and 7 K.

e-p interaction only renormalizes the phonon self-energy without showing a Fano interference in the spectra.

To quantify the superconductivity induced self-energy effects and the e-p interaction strength, we fit the data with $\chi''_{ph}(\omega) \propto 4\omega_0 \Sigma'' [(\omega^2 - \omega_0^2 - 2\omega_0 \Sigma')^2 + 4(\omega_0 \Sigma'')^2]^{-1}$, where ω_0 is the bare phonon frequency, and $\Sigma = \Sigma' + i\Sigma''$ is complex phonon self-energy [24]. Thus, if Σ is small, the mode appears at $\omega_{ph} = \sqrt{\omega_0^2 + 2\omega_0 \Sigma'}$ frequency. The fitting results are displayed in Figs. 4 (b-c) [51].

We calculate the coupling constant $\lambda_{B_{1g}}^\Gamma$ around Γ point [56]: $\lambda = -\kappa \sin u/u$, where $\kappa = [(\Sigma'(7K) - \Sigma'(40K)) - i(\Sigma''(7K) - \Sigma''(40K))]/\omega_{ph}(40K)$ and $u \equiv$

TABLE II. Summary of Raman active phonons mode energies and atomic displacements for $\text{CaKFe}_4\text{As}_4$.

Symmetry	Energy at 40 K	Atomic displacements
$A_{1g}(1)$	67 cm^{-1}	Fe(z)+As(1)(z)+As(2)(z)
$A_{1g}(2)$	185 cm^{-1}	Fe(z)+As(1)(z)+As(2)(z)
$A_{1g}(3)$	286 cm^{-1}	Fe(z)+As(1)(z)+As(2)(z)
$B_{1g}(1)$	213 cm^{-1}	Fe(z)

$\pi + 2i \cosh^{-1}[\omega_{ph}(40K)/2\Delta]$. Using the energy of the strongest pair breaking peak $2\Delta = 135 \text{ cm}^{-1}$, we acquire weak e-p coupling constant $\lambda_{B_{1g}}^\Gamma \approx 0.0015$. The A_{1g} phonons do not show measurable renormalization, Figs. 4(d-e). Therefore, the B_{1g} mode is the only phonon that exhibits the SC induced self-energy effects. Thus, we use $\lambda_{B_{1g}}^\Gamma$ to approximate the total e-p coupling constant λ [57].

In comparison, for a conventional phonon-mediated superconductor MgB_2 with similar $T_c = 39 \text{ K}$, a much larger coupling constant $\lambda = 0.2$ was derived from SC induced phonon renormalization [25]. Thus, for $\text{CaKFe}_4\text{As}_4$, the value λ is far from being sufficient to result in superconductivity with T_c at 35 K.

Conclusions – In summary, we report polarization-resolved Raman spectroscopic study of the single-crystal $\text{CaKFe}_4\text{As}_4$ superconductor with T_c at 35 K.

Above T_c we do not detect Pomeranchuk-like electronic nematic (quadrupole) fluctuations, which implies that the electronic nematicity may not be essential for high- T_c superconductivity in FeSCs.

Below T_c we observe development of a composite coherence feature between 12 and 20 meV in the B_{2g} symmetry channel and a complete suppression of low-frequency spectral weight, which implies that all the FS pockets remain nodeless. We do not detect any sharp in-gap collective modes which were commonly observed for FeSCs which exhibit strong electronic nematic fluctuations.

We also study the SC induced self-energy effects for Raman-active phonons and provide an estimate of the electron-phonon coupling constant $\lambda^\Gamma = 0.0015$, which is very small for a superconductor with T_c at 35 K.

Because both the electronic nematic fluctuations and the superconductivity induced self-energy effects for even-symmetry phononic modes are neglectfully small, we conclude that the spin-fluctuations are responsible for primarily pairing interaction in $\text{CaKFe}_4\text{As}_4$. In this case, the expected pairing symmetry is s_\pm , which is consistent with the observation of the spin-resonance mode at nesting vector (π, π) by inelastic neutron scattering [58].

The spectroscopic work at Rutgers (WZ and GB) was supported by NSF Grant No. DMR-1709161. Crystal growth and characterization at Ames Laboratory (TK and PCC) was supported by the U.S. Department of Energy, Office of Basic Energy Sciences, Division of Materials Sciences and Engineering under Contract No. DE-AC02-07CH11358. W.R.M (crystal growth) was supported by the Gordon and Betty Moore Foundation's EPIQS Initiative through Grant No. GBMF4411.

Note added in revision: While this paper was being reviewed, D. Jost et al. published related Raman study [47]. The authors of Ref. [47] interpret features at 134 cm^{-1} (16.6 meV) and at 50 cm^{-1} (6.2 meV) as Bardasis-Schrieffer (BS) collective modes and argue that appearance of the modes imply subdominant d -wave pair-

ing interactions. We note here that none of the referred features in Raman spectra have a structure of a defined long-lived resonance. As such, assignments to any collective mode is difficult to support. Furthermore, the statement that there exist two independent attractive subdominant XY-symmetry pairing channels is unjustified.

* wz131@physics.rutgers.edu

† girsh@physics.rutgers.edu

- [1] J. Paglione and R. L. Greene, *Nat Phys* **6**, 645 (2010).
- [2] F. Wang and D.-H. Lee, *Science* **332**, 200 (2011).
- [3] A. Chubukov, *Annu. Rev. Condens. Matter Phys.* **3**, 57 (2012).
- [4] R. M. Fernandes, A. V. Chubukov, and J. Schmalian, *Nat. Phys.* **10**, 97 (2014).
- [5] P. J. Hirschfeld, *Comptes Rendus Physique* **17**, 197 (2016).
- [6] Q. Si, R. Yu, and E. Abrahams, *Nat. Rev. Mater.* **1**, 16017 (2016).
- [7] J.-H. Chu, H.-H. Kuo, J. G. Analytis, and I. R. Fisher, *Science* **337**, 710 (2012).
- [8] H.-H. Kuo, J.-H. Chu, J. C. Palmstrom, S. A. Kivelson, and I. R. Fisher, *Science* **352**, 958 (2016).
- [9] T. Shibauchi, A. Carrington, and Y. Matsuda, *Annu. Rev. Condens. Matter Phys.* **5**, 113 (2014).
- [10] Y. Gallais, R. M. Fernandes, I. Paul, L. Chauvière, Y.-X. Yang, M.-A. Méasson, M. Cazayous, A. Sacuto, D. Colson, and A. Forget, *Phys. Rev. Lett.* **111**, 267001 (2013).
- [11] V. K. Thorsmølle, M. Khodas, Z. P. Yin, C. Zhang, S. V. Carr, P. Dai, and G. Blumberg, *Phys. Rev. B* **93**, 054515 (2016).
- [12] S. Lederer, Y. Schattner, E. Berg, and S. A. Kivelson, *Phys. Rev. Lett.* **114**, 097001 (2015).
- [13] M. A. Metlitski, D. F. Mross, S. Sachdev, and T. Senthil, *Phys. Rev. B* **91**, 115111 (2015).
- [14] D. Labat and I. Paul, *Phys. Rev. B* **96**, 195146 (2017).
- [15] M. V. Klein and S. B. Dierker, *Phys. Rev. B* **29**, 4976 (1984).
- [16] T. P. Devereaux and R. Hackl, *Rev. Mod. Phys.* **79**, 175 (2007), and refs therein.
- [17] Y. Gallais, I. Paul, L. Chauvière, and J. Schmalian, *Phys. Rev. Lett.* **116**, 017001 (2016).
- [18] S.-F. Wu, P. Richard, H. Ding, H.-H. Wen, G. Tan, M. Wang, C. Zhang, P. Dai, and G. Blumberg, *Phys. Rev. B* **95**, 085125 (2017).
- [19] T. Böhm, F. Kretzschmar, A. Baum, M. Rehm, D. Jost, R. Hosseinian Ahangharnejhad, R. Thomale, C. Platt, T. A. Maier, W. Hanke, B. Moritz, T. P. Devereaux, D. J. Scalapino, S. Maiti, P. J. Hirschfeld, P. Adelman, T. Wolf, H.-H. Wen, and R. Hackl, ArXiv e-prints (2017), [arXiv:1703.07749](https://arxiv.org/abs/1703.07749).
- [20] F. Kretzschmar, T. Böhm, U. Karahasanovic, B. Muschler, A. Baum, D. Jost, J. Schmalian, S. Caprara, M. Grilli, C. Di Castro, J. G. Analytis, J. H. Chu, I. R. Fisher, and R. Hackl, *Nat. Phys.* **12**, 560 (2016).
- [21] S.-F. Wu, W.-L. Zhang, L. Li, H. B. Cao, H.-H. Kung, A. S. Sefat, H. Ding, P. Richard, and G. Blumberg, ArXiv e-prints (2017), [arXiv:1712.06066](https://arxiv.org/abs/1712.06066).
- [22] S. L. Cooper, M. V. Klein, B. G. Pazol, J. P. Rice, and D. M. Ginsberg, *Phys. Rev. B* **37**, 5920 (1988).
- [23] C. Thomsen, M. Cardona, B. Gegenheimer, R. Liu, and A. Simon, *Phys. Rev. B* **37**, 9860 (1988).
- [24] R. Zeyher and G. Zwiczak, *Z. Phys. B* **78**, 175 (1990).
- [25] A. Mialitsin, B. S. Dennis, N. D. Zhigadlo, J. Karpinski, and G. Blumberg, *Phys. Rev. B* **75**, 020509 (2007).
- [26] W. R. Meier, T. Kong, U. S. Kaluarachchi, V. Taufour, N. H. Jo, G. Drachuck, A. E. Böhmer, S. M. Saunders, A. Sapkota, A. Kreyssig, M. A. Tanatar, R. Prozorov, A. I. Goldman, F. F. Balakirev, A. Gurevich, S. L. Bud'ko, and P. C. Canfield, *Phys. Rev. B* **94**, 064501 (2016).
- [27] A. Iyo, K. Kawashima, T. Kinjo, T. Nishio, S. Ishida, H. Fujihisa, Y. Gotoh, K. Kihou, H. Eisaki, and Y. Yoshida, *J. Amer. Chem. Soc.* **138**, 3410 (2016).
- [28] W. R. Meier, T. Kong, S. L. Bud'ko, and P. C. Canfield, *Phys. Rev. Materials* **1**, 013401 (2017).
- [29] R. Yang, Y. Dai, B. Xu, W. Zhang, Z. Qiu, Q. Sui, C. C. Homes, and X. Qiu, *Phys. Rev. B* **95**, 064506 (2017).
- [30] K. Kawashima, S. Ishida, H. Fujihisa, Y. Gotoh, K. Kihou, Y. Yoshida, H. Eisaki, H. Ogino, and A. Iyo, *J. Phys. Chem. Lett.* **9**, 868 (2018).
- [31] W. R. Meier, Q.-P. Ding, A. Kreyssig, S. L. Bud'ko, A. Sapkota, K. Kothapalli, V. Borisov, R. Valentí, C. D. Batista, P. P. Orth, R. M. Fernandes, A. I. Goldman, Y. Furukawa, A. E. Böhmer, and P. C. Canfield, *npj Quantum Materials* **3**, 5 (2018).
- [32] U. S. Kaluarachchi, V. Taufour, A. Sapkota, V. Borisov, T. Kong, W. R. Meier, K. Kothapalli, B. G. Ueland, A. Kreyssig, R. Valentí, R. J. McQueeney, A. I. Goldman, S. L. Bud'ko, and P. C. Canfield, *Phys. Rev. B* **96**, 140501 (2017).
- [33] L. Xiang, W. R. Meier, M. Xu, U. S. Kaluarachchi, S. L. Bud'ko, and P. C. Canfield, *Phys. Rev. B* **97**, 174517 (2018).
- [34] V. Cvetkovic and O. Vafek, *Phys. Rev. B* **88**, 134510 (2013).
- [35] J. Hu and N. Hao, *Phys. Rev. X* **2**, 021009 (2012).
- [36] Y. A. Pomeranchuk, *Sov. Phys. JETP* **8**, 361 (1958).
- [37] M. Khodas, A. V. Chubukov, and G. Blumberg, *Phys. Rev. B* **89**, 245134 (2014).
- [38] S. Maiti, A. V. Chubukov, and P. J. Hirschfeld, *Phys. Rev. B* **96**, 014503 (2017).
- [39] F. Lochner, F. Ahn, T. Hickel, and I. Eremin, *Phys. Rev. B* **96**, 094521 (2017).
- [40] J. Cui, Q.-P. Ding, W. R. Meier, A. E. Böhmer, T. Kong, V. Borisov, Y. Lee, S. L. Bud'ko, R. Valentí, P. C. Canfield, and Y. Furukawa, *Phys. Rev. B* **96**, 104512 (2017).
- [41] $\mu\nu$ is short for $\bar{Z}(\mu\nu)Z$ in Porto's notation.
- [42] The background is determined from the X'Y' symmetry scattering intensity after subtracting the B_{1g} phonon, see supplement I in [59].
- [43] G. Blumberg, A. Mialitsin, B. Dennis, N. Zhigadlo, and J. Karpinski, *Physica C: Superconductivity* **456**, 75 (2007).
- [44] C. Sauer and G. Blumberg, *Phys. Rev. B* **82**, 014525 (2010).
- [45] D. Mou, T. Kong, W. R. Meier, F. Lochner, L.-L. Wang, Q. Lin, Y. Wu, S. L. Bud'ko, I. Eremin, D. D. Johnson, P. C. Canfield, and A. Kaminski, *Phys. Rev. Lett.* **117**, 277001 (2016).
- [46] M. V. Klein, *Phys. Rev. B* **82**, 014507 (2010).
- [47] D. Jost, J.-R. Scholz, U. Zweck, W. R. Meier, A. E. Böhmer, P. C. Canfield, N. Lazarević, and R. Hackl, *Phys. Rev. B* **98**, 020504 (2018).

- [48] A. V. Chubukov, I. Eremin, and M. M. Korshunov, *Phys. Rev. B* **79**, 220501 (2009).
- [49] P. G. Klemens, *Phys. Rev.* **148**, 845 (1966).
- [50] J. Menéndez and M. Cardona, *Phys. Rev. B* **29**, 2051 (1984).
- [51] $\omega_{ph}(T) = \omega_{ph}(0) - \omega_1(1 + 2/(\exp(\omega_{ph}(0)/k_B T) - 1))$, $\Sigma''(T) = \Sigma''(0) + \Gamma_1(1 + 2/(\exp(\omega_{ph}(0)/k_B T) - 1))$ are used to fit $\omega_{ph}(T)$ and $\Sigma''(T)$ for the normal state [49]. The dashed curves in Figs. 4b-c are plotted with the fitting result $\omega_{ph}(0) = 216.0 \pm 0.1 \text{ cm}^{-1}$, $\omega_1 = 3.1 \pm 0.1 \text{ cm}^{-1}$, $\Sigma''(0) = 2.2 \pm 0.3 \text{ cm}^{-1}$, and $\Gamma_1 = 0.6 \pm 0.3 \text{ cm}^{-1}$.
- [52] B. Friedl, C. Thomsen, and M. Cardona, *Phys. Rev. Lett.* **65**, 915 (1990).
- [53] K. F. McCarty, H. B. Radousky, J. Z. Liu, and R. N. Shelton, *Phys. Rev. B* **43**, 13751 (1991).
- [54] G. Blumberg, M. V. Klein, L. Börjesson, R. Liang, and W. N. Hardy, *J. Supercond.* **7**, 445 (1994).
- [55] C. Thomsen and M. Cardona, “Raman scattering in high-*T*c superconductors,” in *Physical Properties of High Temperature Superconductors I*, Chap. 8, pp. 409–507.
- [56] C. O. Rodriguez, A. I. Liechtenstein, I. I. Mazin, O. Jepsen, O. K. Andersen, and M. Methfessel, *Phys. Rev. B* **42**, 2692 (1990).
- [57] Because the electron-phonon coupling strength is not expected to change markedly with phonon dispersion, λ_{B1g}^{Γ} can be used to approximate the total e-p coupling.
- [58] K. Iida, M. Ishikado, Y. Nagai, H. Yoshida, A. D. Christianson, N. Murai, K. Kawashima, Y. Yoshida, H. Eisaki, and A. Iyo, *J. Phys. Soc. Jpn.* **86**, 093703 (2017).
- [59] W.-L. Zhang, S.-F. Wu, S. Kasahara, T. Shibauchi, Y. Matsuda, and G. Blumberg, ArXiv e-prints (2017), [arXiv:1710.09892](https://arxiv.org/abs/1710.09892).